

Assessing the correlated electronic structure of lanthanum nickelates

Frank Lechermann

European XFEL, Holzkoppel 4, 22869 Schenefeld, Germany
Center for Computational Quantum Physics, The Flatiron Institute, 162 5th Avenue, New York, NY 10010, USA

Abstract. The series of nickel-oxide compounds LaNiO_3 (formal $\text{Ni}(d^7)$), La_2NiO_4 (formal $\text{Ni}(d^8)$) and LaNiO_2 (formal $\text{Ni}(d^9)$) is investigated by first-principles many-body, using a combination of density functional theory, self-interaction correction and dynamical mean-field theory. The characteristics of these different nickelates, in good agreement with available experimental data, is revealed by employing a compound-independent choice for the local Coulomb interactions. The dichotomy within the low-energy dominant $\text{Ni-}e_g$ sector of $\{d_{z^2}, d_{x^2-y^2}\}$ kind is rising with growing $\text{Ni}(3d)$ filling across the series. An intermediate-coupling scheme for spin-polarized calculations is introduced, which leads to very weak Ni ordered moments for the infinite-layer compound LaNiO_2 in contrast to the robust-moment system La_2NiO_4 .

1. Introduction

Since the earliest days of studies on strongly correlated condensed matter [1], research on nickel-oxide compounds has ever been an important aspect. But it just recently received a further boost when superconductivity was discovered in thin films of Sr-doped infinite-layer NdNiO_2 [2]. Nickelates are key examples of late transition-metal oxides where the t_{2g} manifold of the $\text{Ni}(3d)$ shell is in most cases filled, and the e_g subshell plays the major active role. While in neighboring (layered) cuprates that latter subshell physics reduces in the most interesting cases to an effective one-band/orbital picture [3], the multiorbital character usually remains intact for nickelates. Rich phase diagrams with various competing orders are the result of this scenario (see e.g. Ref. [4] and references therein).

Concerning the research over the last 40 years, one may roughly group the respective dominant nickelate studies compound-wise into three areas. First, from traditional work on Mott insulators [1] and the apparent structural affinity to high- T_c cuprates [5], in the 1980s and early 1990s, the emphasis was on formal $\text{Ni}(3d^8)$ materials, e.g. NiO [6–9] and La_2NiO_4 [10–15]. Starting from the early 1990s until later 2010s, main attention shifted towards formal $\text{Ni}(3d^7)$ compounds, mainly to the rare-earth (RE) perovskite(-like) RENiO_3 series [16]. Though discussed early on [17], work on formal $\text{Ni}(3d^9)$ systems heavily increased after the finding of superconducting infinite-layer nickelates in the mid of 2019 [2].

In this work we want to provide an theoretical overview over these different formal $\text{Ni}(3d^{n=7,8,9})$ classes, by focussing on one representative material from each class and describing them within an advanced first-principles many-body approach. Goal is to identify the key features of each class, to look for coherent theoretical settings and similarities across the classes, and to weigh the quality of the description for this wider nickelate family. To provide largest coherence from the ligand side, we choose the following series of lanthanum nickelates for the investigation: LaNiO_3 (formal d^7), La_2NiO_4 (formal d^8) and LaNiO_2 (formal d^9). While LaNiO_3 is well known as a paramagnetic metal down to lowest temperatures and La_2NiO_4 as antiferromagnetic Mott/charge-transfer insulator over a wide temperature range, the definite electronic and magnetic characterization of LaNiO_2 is still a matter of intense debate. The role of an apparent self-doping band [18–20] in the latter compound complicates the correlation problem.

It will be shown that for a rather coherent setting, our theoretical modelling delivers good agreement with the key characterization and long-standing experimental results for LaNiO_3 and La_2NiO_4 . For the same setting, we identify in the case of challenging LaNiO_2 an overall weak-metallic state (due to self doping) accompanied by an orbital-selective Mott-insulating $\text{Ni}-e_g$ sector, very similar to recent findings for NdNiO_2 .

2. Methodology

2.1. General framework

We utilize the DFT+*sic*DMFT scheme [21], a charge self-consistent combination [22–24] of density functional theory (DFT), self-interaction correction (SIC) and dynamical mean-field theory (DMFT), to assess the correlated electronic structure of LaNiO_3 , La_2NiO_4 and LaNiO_2 . A mixed-basis pseudopotential (MBPP) code [25–27] takes care

of the DFT part in the local density approximation (LDA). To consider correlation effects beyond LDA driven by the oxygen sites in the given late transition-metal oxides, Coulomb interactions on oxygen are described within SIC, and are incorporated in the O pseudopotential [28–30]. The SIC is applied to the O(2s) and the O(2p) orbitals via weight factors w_p (see Ref. [30] for details). While the O(2s) orbital is by default fully corrected with $w_p = 1.0$, the adequate choice [21, 30] $w_p = 0.8$ is used for O(2p) orbitals. The La(4f) states are frozen in the pseudopotential core, as they supposed to be empty and appear especially irrelevant for the key physics of the superconducting nickelates [31–33]. The full Ni(3d) shell is used to construct the correlated subspace of the DMFT impurity problem via the projected-local orbitals formalism [34]. The projection is performed on the minimal set of Kohn-Sham (KS) states above the dominant O(2s) bands, associated with O(2p) and Ni(3d). For LaNiO₂, the self-doping band is additionally included in the projection sphere [20, 35, 36]. A five-orbital rotational-invariant Slater Hamiltonian, parametrized by a Hubbard U and a Hund’s exchange J_H , is active in the correlated subspace. If not otherwise stated, we stick to $U = 10$ eV and $J_H = 1$ eV as in previous nickelate studies [20, 21, 35, 36]. One main goal of the present work is to check whether such a compound-independent choice of local Coulomb parameters may satisfyingly describe a wider range of different nickelates.

2.2. Spin-polarized calculations

The description of ordered magnetism in first-principles many-body calculations of DFT+DMFT type leaves room for methodological interpretation [37]. As a hybrid scheme, the spin polarization can be handled in different ways. Allowing for local ordered spin moments in the DMFT part to investigate possible magnetically ordered phases is definitely adequate (e.g. Ref. [38]). There is common agreement that explicit correlation effects in partially-filled d - or f -shells are a crucial ingredient of most spin-ordering phenomena in condensed matter. An additional treatment also in the DFT part may have pros and cons. On the positive side, a strong itinerant aspect of spin polarization, relevant for some weakly/moderately correlated compounds, might be better included. Also short-range ‘ligand-coupling’ effects could be more realistically covered by a DFT-based spin polarization of the charge density. On the negative side, the double-counting construction is not well suited for the explicit spin-polarization aspect. As a result, an often strong, static and temperature-independent exchange coupling within DFT dominates the physics, and subtle correlation effects in the magnetization are easily outshined. For instance, computation of Curie temperatures is more or less impossible with a full spin-polarized DFT+DMFT scheme. Since most DFT+DMFT studies aim at correlations effect at strong coupling (i.e. close to a Mott-critical regime), therefore treating spin polarization only on the DMFT and not on the DFT level, has become the standard method for describing magnetically ordered phases.

In contrast to the both restrictive routes, i.e. DFT part spin-polarized or not, we here want to suggest an alternative way of handling spin polarization in the given context of our nickelate study, which we term *intermediate coupling (IC)* scheme. Key idea is to neglect only the local DFT part of spin polarization, since that one should for sure be comprehensively covered by the spin-polarized DMFT self-energies. The remaining strictly itinerant DFT charge-density terms may still carry finite spin polarization.

In the mixed-basis pseudopotential approach [25], the KS wave function for Bloch

vector \mathbf{k} , band ν and spin $\sigma = \uparrow, \downarrow$ is expanded into plane waves (pw) and localized functions (lf), reading

$$\psi_{\mathbf{k}\nu\sigma}(\mathbf{r}) = \frac{1}{\sqrt{\Omega_c}} \sum_{\mathbf{G}} \psi_{\mathbf{G}}^{\mathbf{k}\nu\sigma} e^{i(\mathbf{k}+\mathbf{G})\cdot\mathbf{r}} + \sum_{\gamma lm} \beta_{\gamma lm}^{\mathbf{k}\nu\sigma} \phi_{\gamma lm}^{\mathbf{k}}(\mathbf{r}) , \quad (1)$$

where Ω_c is the unit-cell volume, \mathbf{G} a reciprocal-lattice vector, γ labels an atom in the unit cell and lm are the usual angular-momentum quantum numbers. The localized functions are given by

$$\phi_{\gamma lm}(\mathbf{r}) = i^l g_{\gamma l}(r) K_{lm}(\hat{\mathbf{r}}) , \quad (2)$$

$$\phi_{\gamma lm}^{\mathbf{k}}(\mathbf{r}) = \sum_{\mathbf{T}} e^{i\mathbf{k}\cdot(\mathbf{T}+\mathbf{R}_{\gamma})} \phi_{\gamma lm}(\mathbf{r} - \mathbf{T} - \mathbf{R}_{\gamma}) , \quad (3)$$

whereby g is a radial function, K a cubic-harmonic function and \mathbf{T} a lattice vector. Accordingly, the KS electronic charge density $\rho(\mathbf{r})$ consists of three terms, i.e.

$$\rho_{\sigma}(\mathbf{r}) = \sum_{\mathbf{k}\nu} f_{\mathbf{k}\nu\sigma} |\psi_{\mathbf{k}\nu\sigma}(\mathbf{r})|^2 = \rho_{\sigma}^{\text{pw,pw}}(\mathbf{r}) + \rho_{\sigma}^{\text{pw,lf}}(\mathbf{r}) + \rho_{\sigma}^{\text{lf,lf}}(\mathbf{r}) . \quad (4)$$

For instance, the purely-local third term $\rho^{\text{lf,lf}}$ does not carry any plane-wave part and reads

$$\rho_{\sigma}^{\text{lf,lf}}(\mathbf{r}) = \sum_{\mathbf{k}\nu\sigma} f_{\mathbf{k}\nu\sigma} \left| \sum_{\gamma lm} \beta_{\gamma lm}^{\mathbf{k}\nu\sigma} \phi_{\gamma lm}^{\mathbf{k}}(\mathbf{r}) \right|^2 = \sum_{\mathbf{T}, \gamma lm} \rho_{\gamma lm\sigma}^{\text{lf,lf}}(r') K_{lm}(\hat{\mathbf{r}}') , \quad (5)$$

with $\mathbf{r}' = \mathbf{r} - \mathbf{T} - \mathbf{R}_{\gamma}$, and hence can be understood as an expansion into cubic harmonics.

In the standard DFT+DMFT calculation for magnetically ordered phases of correlated materials, all terms in eq. (4) are spin-independent from a nonmagnetic KS treatment in each DFT step. Instead, we here suggest to perform a spin-polarized KS calculation in each DFT step and the following representation of the associated charge density

$$\rho_{\sigma}^{\text{DFTpart}}(\mathbf{r}) = \rho_{\sigma}^{\text{pw,pw}}(\mathbf{r}) + \rho_{\text{av}}^{\text{pw,lf}}(\mathbf{r}) + \rho_{\text{av}}^{\text{lf,lf}}(\mathbf{r}) , \quad (6)$$

with

$$\rho_{\text{av}}^{\text{pw,lf}}(\mathbf{r}) = \frac{1}{2} \left(\rho_{\uparrow}^{\text{pw,lf}}(\mathbf{r}) + \rho_{\downarrow}^{\text{pw,lf}}(\mathbf{r}) \right) , \quad (7)$$

$$\rho_{\text{av}}^{\text{lf,lf}}(\mathbf{r}) = \frac{1}{2} \left(\rho_{\uparrow}^{\text{lf,lf}}(\mathbf{r}) + \rho_{\downarrow}^{\text{lf,lf}}(\mathbf{r}) \right) . \quad (8)$$

Thus the fully local (lf,lf) term, as well as the semi-local (pw,lf) term are spin-averaged in the DFT part. Note that a coupling between local and plane-wave part is already facilitated via the, then spin-dependent, projected-local orbitals $\sim \langle \phi_{\gamma lm} | \psi_{\mathbf{k}\nu\sigma} \rangle$ in the construction of the correlated subspace [34]. It therefore proves indeed adequate to also average the (pw,lf) term in eq. (4), since the DMFT-relevant and therefore correlation-relevant intermixing between local and full Hilbert space is already established at a different place in the complete DFT+DMFT framework [24].

Using representation (6) on the pure DFT level results of course in a self-consistent vanishing of a possible ordered moment for correlated materials of interest. However in DFT+(sic)DMFT, the many-body part will reinject spin polarization within the IC scheme, eventually with a more subtle and balanced linkage between the weakly and strongly correlated aspects of magnetic ordering.

2.3. Crystal data and further computational settings

All structural data for the La nickelates are taken from experiment. The LaNiO_3 compound crystallizes in a two-formula-unit cell with rhombohedral $R\bar{3}c$ space group, and we used the data by Zhang *et al.* [39]. The structure is very similar to, but deviates slightly from a basic perovskite structure (see top of Fig. 1a). The Ni site is in an octahedral coordination and the Ni-O bond length amounts to $d_{\text{Ni}}^{\text{O}} = 1.929 \text{ \AA}$. The same coordination holds also for Ni in La_2NiO_4 , which is the single-layer $p = 1$ compound of the Ruddlesden-Popper series $\text{La}_{p+1}\text{Ni}_p\text{O}_{3p+1}$ and basically iso-structural to the famous high- T_c cuprate La_2CuO_4 as well as the famous low- T superconducting ruthenate Sr_2RuO_4 . At ambient temperature, La_2NiO_4 crystallizes in the orthorhombic $Bmab$ structure (see mid of Fig. 1a) with a two-formula-unit cell. The in-plane Ni-O distance amounts to $d_{\text{Ni}}^{\text{O,ip}} = 1.948 \text{ \AA}$, while the out-of-plane distance to the apical oxygen reads $d_{\text{Ni}}^{\text{O,oop}} = 2.267 \text{ \AA}$. Above $T \sim 770 \text{ K}$ the compound transforms to the simpler tetragonal $I4/mmm$ structure. Below $T \sim 80 \text{ K}$ the system transforms to a new tetragonal phase with $P4_2/ncm$ symmetry, however that phase is not considered in the present work. All lattice data on La_2NiO_4 is taken from the work by Rodriguez-Carvajal *et al.* [40]. Finally, the LaNiO_2 compound with $P4/mmm$ space group cannot be grown in single-crystal form, but exists as polycrystals [41] and in thin films on SrTiO_3 [32, 33]. This infinite-layer structure consists of NiO_2 layers with $d_{\text{Ni}}^{\text{O}} = 1.980 \text{ \AA}$ and missing apical oxygen (see bottom of Fig. 1a). We use the lattice data for the single-phase model from Hayward *et al.* [41]. The general increase of d_{Ni}^{O} from LaNiO_3 to La_2NiO_4 and LaNiO_2 may be associated with the expected lowering of the Ni oxidation state.

For the DFT+*sic*DMFT calculations we utilize a plane-wave cutoff $E_{\text{cut}} = 16 \text{ Ry}$ and a $13 \times 13 \times 13$ k -point mesh for LaNiO_2 . The respective k -point mesh for the other structure is accordingly tailored to yield the identical k -point density. Localized functions in the MBPP formalism are introduced for $\text{La}(5d)$, $\text{Ni}(3d)$ as well as $\text{O}(2s, 2p)$. Continuous-time quantum Monte Carlo in hybridization expansion [42] as implemented in the TRIQS code [43, 44] is utilized to solve the quantum-impurity problem. The fully-localized-limit double-counting scheme [45] is applied. Maximum-entropy [46] and Padé [47] methods are employed for the analytical continuation from Matsubara space onto the real-frequency axis. Paramagnetic (PM) calculations are performed for LaNiO_3 . In the case of La_2NiO_4 and LaNiO_2 , both, paramagnetic and antiferromagnetic (AFM) phases are investigated, for details see the corresponding sections 4 and 5.

3. General electronic structure aspects

Before discussing individual aspects of each of the studied nickelate compounds, let us start with an overview of the correlated structure when lowering the Ni 'oxidation potential' from LaNiO_3 via La_2NiO_4 to LaNiO_2 . Figure 1b displays from top to bottom the total and site-orbital-projected spectral function $A(\omega)$ for the three oxides. Note again that the local Coulomb parameters $U = 10 \text{ eV}$ and $J_{\text{H}} = 1 \text{ eV}$ are kept identical for each compound.

The slightly-distorted perovskite LaNiO_3 is the metallic end member of the RENiO_3 series. Formally, nickel is in the $3+$ oxidation state, i.e. a local $3d^7(t_{2g}^6 e_g^1)$ configuration would hold. Yet from the present calculations, Ni is closer to a $3d^8(t_{2g}^6 e_g^2)$ configuration with a ligand hole on oxygen, i.e. a $3d^8\bar{L}$ state. In detail, according to

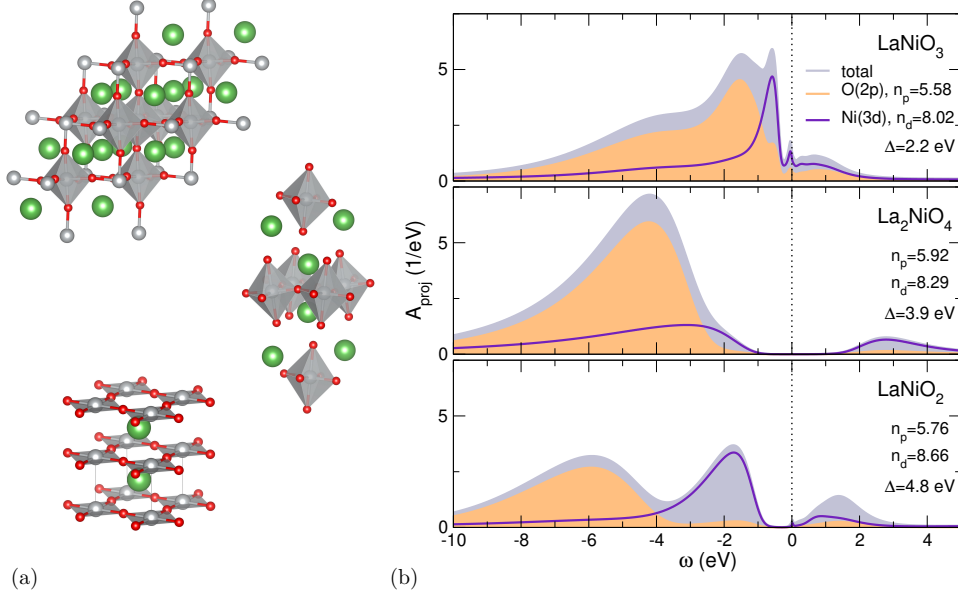


Figure 1. Structural and spectral overview for the nickelate compounds LaNiO₃, La₂NiO₄ and LaNiO₂. (a) Top to bottom: ambient-temperature crystal structure of the compounds. LaNiO₃: rhombohedral $R\bar{3}c$; La₂NiO₄ orthorhombic $Bmab$; LaNiO₂: tetragonal $P4/mmm$. La (green), Ni (grey) and oxygen (red). (b) Top to bottom: DFT+sicDMFT total and projected spectral function for PM-LaNiO₃, AFM-La₂NiO₄ and PM-LaNiO₂ at $T = 193$ K, respectively. The values for n_p and n_d refer to the O(2p) and Ni(3d) filling as obtained from integrating $A_{\text{proj}}(\omega)$. The respective charge-transfer energy Δ is computed within DFT+sic (see text).

the projected spectral function, the average O(2p) filling per oxygen site $n_p = 5.58$ translates into about 1.2 holes per unit cell. A significant oxygen hole density can also easily be observed from substantial O(2p) spectral weight above the Fermi level ε_F . This finding is in line with previous works [48–54] that emphasize the preference for oxygen-hole formation in LaNiO₃ and presumably in further formal-3d⁷ nickelates. Under these circumstances, the (effective) charge-transfer energy $\Delta_{\text{(eff)}}$ should be small or even negative [4]. We here define $\Delta = \varepsilon_d - \varepsilon_p$ as obtained from DFT+sic, i.e. nonmagnetic DFT calculations with SIC on oxygen, and $\varepsilon_{d,p}$ as the respective centers of the associated Ni(3d) and O(2p) projected-local-orbital bands. The resulting $\Delta_{\text{LaNiO}_3} = 2.2$ eV is indeed rather small.

The Ni(3d) filling n_d raises in La₂NiO₄ and the number of oxygen holes is comparatively small. The Ni²⁺ state with 3d⁸ configuration is indeed closest to reality. The system is an AFM insulator with a charge gap Δ_g of about 4 eV, in line with experiment [55]. However note that compared to prototypical NiO [21], the valence-band-maximum states are of stronger Ni(3d) character. The charge-transfer energy is computed as $\Delta_{\text{La}_2\text{NiO}_4} = 3.9$ eV, significantly larger than for LaNiO₃ and also in good accordance with experimental estimates [15]. With $\Delta \ll U$ and $\Delta \sim \Delta_g$ the system may be classified as a charge-transfer insulator.

The LaNiO₂ compound with n_d closer to 3d⁹ has apparently a more subtle electronic structure than given by an obvious metal or insulator. The Ni(3d) states are

nearly gapped, but minor spectral weight remains at the Fermi level. The oxygen-hole content is non-negligible but not as strong as for LaNiO_3 ; there are only about 0.5 holes per unit cell. However note that the here provided fillings derived from the *projected* spectral function may differ somewhat from values extracted from the *local* spectral function. The values n_d^{loc} associated with the latter function read $\{7.95, 8.15, 8.84\}$ for LaNiO_3 , La_2NiO_4 and LaNiO_2 . The infinite-layer compound shows the largest charge-transfer energy $\Delta_{\text{LaNiO}_2} = 4.8 \text{ eV}$ among the here studied nickelates. In line with the increase of Δ with a shrinking formal oxidation state, the $\text{O}(2p)$ levels shift to deeper energies with rising $\text{Ni}(3d)$ filling.

In the following three subsections, we will discuss the specific features of the individual compounds in more detail.

4. LaNiO_3

Down to low temperature, the LaNiO_3 compound remains in a strongly correlated metallic state [16], with an experimental mass renormalization m^*/m of about 3–4 [56,57]. There have already been various DFT+DMFT accounts for this nickelate, however most studies focus on a two-orbital $\text{Ni-}e_g$ correlated subspace, and only few treat the full five-orbital $\text{Ni}(3d)$ shell as correlated within DMFT [58,59].

Based on our calculations utilizing the five-orbital correlated subspace, Fig. 2b displays the \mathbf{k} -resolved spectral function along high-symmetry lines in the Brillouin zone of the $R\bar{3}c$ structure (see Fig. 2a). The $\text{Ni-}e_g$ orbitals are degenerate and two corresponding bands cross the Fermi level, showing a DFT bandwidth of $\sim 2.5 \text{ eV}$. The $\text{Ni-}t_{2g}$ orbitals are mostly filled and the associated bands remain below ε_F [58]. Compared to the DFT dispersion, there is a significant band renormalization for the low-energy $\text{Ni-}e_g$ dominated bands. Figure 2c documents the U dependence of the local $\text{Ni-}e_g$ self-energy part $\text{Im}\Sigma(i\omega_n)$ for small Matsubara frequencies ω_n , with the extracted $m^*/m_{\text{LDA}} = (1 - \partial \text{Im}\Sigma / \partial \omega_n|_{\omega_n \rightarrow 0})^{-1}$ in this orbital basis. It is seen that the effective mass is indeed closest to the experimental regime for our general choice $U = 10 \text{ eV}$, while it remains too small for a lower on-site Coulomb interaction. Note that the actual effective mass in the band basis, which strictly speaking should be the one for comparison with experiment, is lower and amounts to $m^*/m_{\text{LDA band}} \sim 2.5$. Thus, even a rather large U value does not quite lead to a perfect-matching magnitude for the experimental $\text{Ni-}e_g$ band renormalization. For instance, non-local spin fluctuations could be a further source for additional renormalization effects.

The explicit local $\text{Ni-}e_g$ occupation amounts exactly to two electrons, i.e. both the $\text{Ni-}d_{z^2}$ and $\text{Ni-}d_{x^2-y^2}$ orbital each host one electron. This becomes also clear from the local spectral function shown in the bottom panel of Fig. 2, where the half-filled e_g states give rise to a renormalized quasiparticle peak (A) at the Fermi level. The total $A(\omega)$ exhibits further peaks at -0.6 eV (B), -1.5 eV (C) and -4.2 eV (D) in the occupied part of the spectrum. Peak B is associated with $\text{Ni-}t_{2g}$, C with $\text{O}(2p)$ and D with $\text{O}(2p)/\text{Ni}(3d)$ -Hubbard-band. The prominent two-peak $\text{O}(2p)$ structure at higher energies below the dominant $\text{Ni}(3d)$ part, supposedly due to the intricate $3d^8\bar{L}$ ground state, can already be drawn from Fig. 1. Though there is overall agreement with photoemission data [16], there are slight differences for the peak positions; in experiment, especially peak C is located at deeper -2.4 eV . Lowering the U value shifts C to somewhat to higher negative energies, but still not reaching the experimental location. But as discussed before, the quasiparticle e_g renormalization

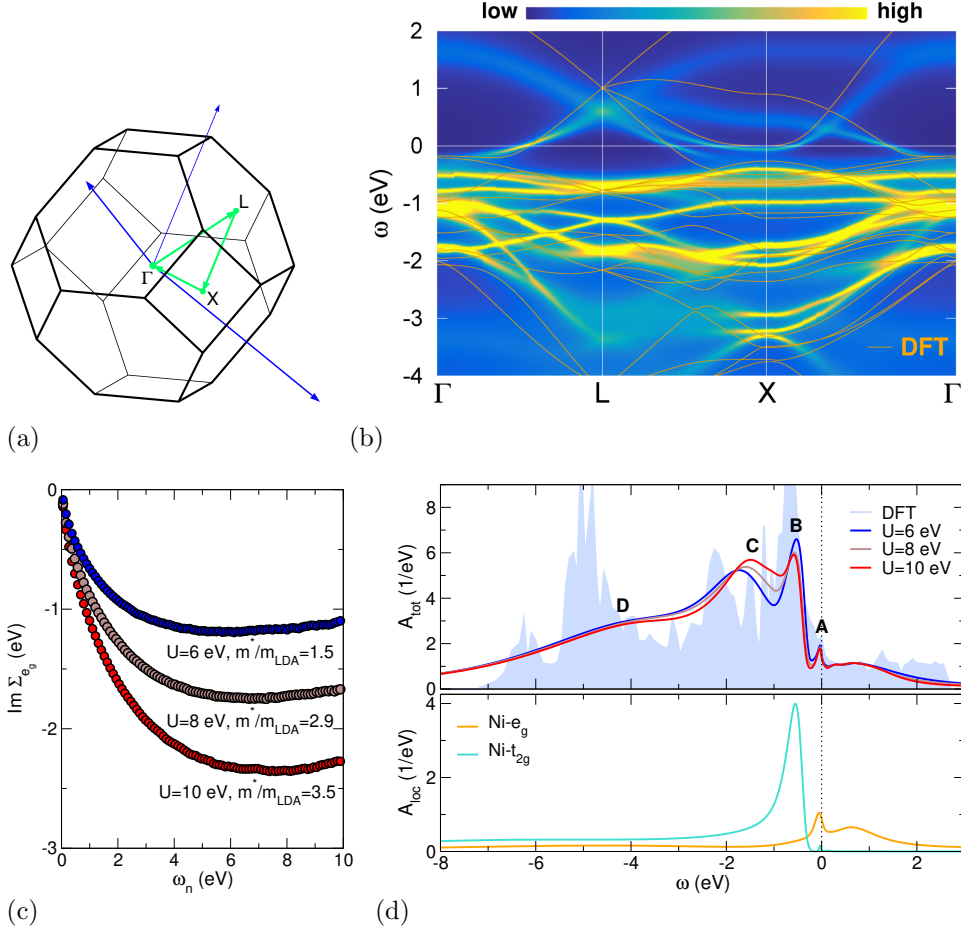


Figure 2. Data for LaNiO₃. (a) Brillouin zone with high-symmetry lines for the $R\bar{3}c$ structure. (b-d) DFT+sicDMFT results for $T = 193$ K: (b) \mathbf{k} -resolved spectral function with comparison to DFT dispersion; (c) imaginary part of the Ni- e_g self-energy for different U values, yielding varying effective masses; (d) \mathbf{k} -integrated total spectrum (top) and local Ni(3d) spectrum (bottom).

becomes too small for smaller U . Notably, the plain DFT spectrum places the main part of peak C in better accordance with experiment. In summary, DFT+sicDMFT provides a good description of LaNiO₃ for the chosen set of Coulomb parameters, however, some questions remain concerning correlation strength and the general electronic spectrum. Albeit originally-thought a rather unspectacular compound, a very good description/understanding of the LaNiO₃ electronic structure turns out still challenging [60].

5. La₂NiO₄

As the natural nickelate analog to the canonical high- T_c cuprate La₂CuO₄, experimentally, the La₂NiO₄ compound has been studied extensively in the past (see

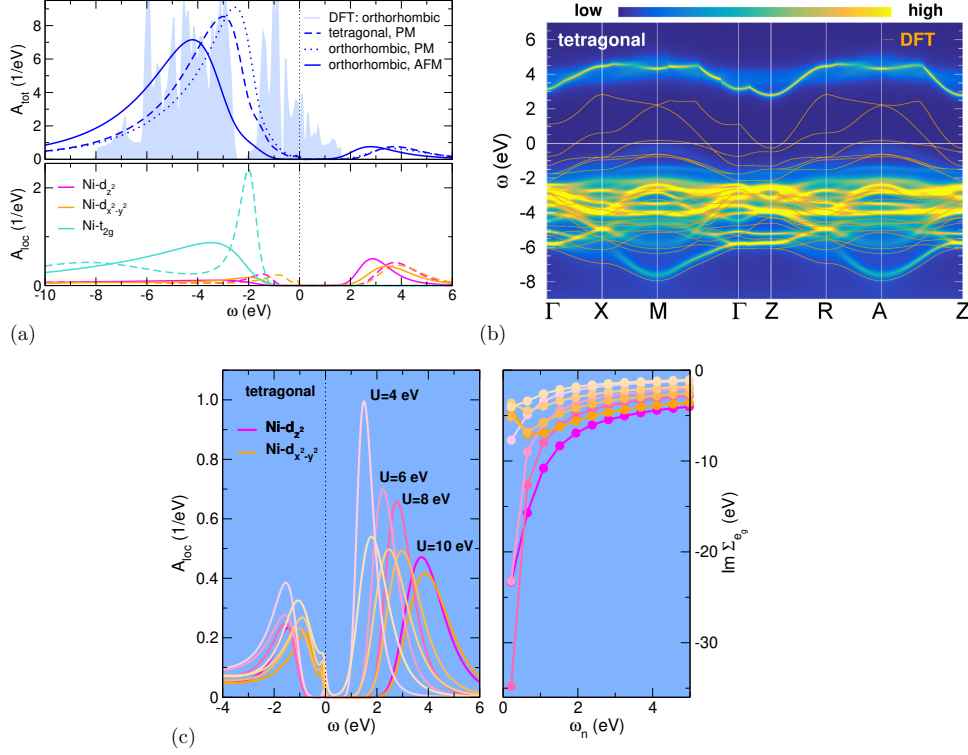


Figure 3. DFT+sicDMFT data for La_2NiO_4 . (a) k -integrated total spectrum (top) and local Ni(3d) spectrum (bottom) for different structural and magnetic cases at $T = 193$ K. (b) k -resolved spectral function for the tetragonal phase at $T = 800$ K with comparison to DFT dispersion. (c) Local Ni- e_g spectral function (left) and imaginary part of the Ni- e_g self-energies (right) for different U values in the tetragonal phase at $T = 800$ K.

e.g. [4] and references therein for the phenomenology with hole doping). However to our surprise, while there are standard-DFT [13,61], DFT+U [62] and meta generalized-gradient approximation [63] studies, we could not find an in-depth realistic-DMFT investigation for this material in the literature. This section is hence also devoted to fill this void.

From an experimental point of view, ensuring the exact stoichiometry for the undoped compound, especially in view of the oxygen content [64,65], appears the most critical issue in defining the correct electronic phases. Here, we do not delve into the intriguing question of defect behavior at nominal stoichiometry, but discuss the perfectly-ordered system.

The orthorhombic compound at ambient and lower temperature is described metallic in nonmagnetic DFT (see Fig. 3a). By imposing strong electronic correlations and additional antiferromagnetic order, La_2NiO_4 is transferred into a Mott-insulating state with a sizable charge gap of ~ 4 eV. That latter value and the associated electronic spectrum (full line in top panel of Fig. 3a) are in very good agreement with data from photoelectron spectroscopy [55]. There is a prominent and broad peak centered at -4 eV, mainly constituted by $O(2p)$ (cf. mid panel of Fig. 1b). The upper

Hubbard-band edges of Ni- e_g character are responsible for a shoulder at -2 eV. While the Ni- t_{2g} orbitals are once more completely filled, Ni- $d_{x^2-y^2}$ and Ni- d_{z^2} both host one electron, i.e. $\{n_{z^2}, n_{x^2-y^2}\} = \{1.07, 1.09\}$, respectively. The ordered Ni moment in the standard G-type AFM phase turns out $m_{\text{Ni}} = 1.65 \mu_B$ at $T = 193$ K from our IC-scheme calculations, with an equal share of spin polarization between both Ni- e_g orbitals. Thus the Ni moment deviates significantly from the value associated with a saturated $S = 1$ spin, but is again in very good agreement with experimental values [40, 66]. Note that from neutron diffraction the Néel temperature is located at $T_N = 330$ K [40]. It is however important to realize that the magnetic order is not decisive for establishing the insulating state.

The high-temperature phase of La_2NiO_4 has been a matter of debate in the past. Transport studies [67] motivated a (bad-)metallic scenario for the tetragonal phase of La_2NiO_4 , i.e. some kind of metal-to-insulator transition with rising temperature. Goodenough and coworkers [10, 68] suggested an orbital-selective Mott transition upon heating, whereby the Ni- d_{z^2} states remain insulating but the Ni- $d_{x^2-y^2}$ states become metallic. From a structural point of view, the absence of the further extension and rotation of the NiO_6 octahedron known within the $Bmab$ phase, leads to a weaker splitting between both e_g states [61]. The DFT crystal-field splitting $\Delta_{\text{cf}} = \varepsilon_{z^2} - \varepsilon_{x^2-y^2}$ amounts to 66 meV in the orthorhombic phase and to 38 meV in the tetragonal phase. Additionally, while the total Ni- e_g bandwidth in the tetragonal phase amounts to ~ 2.8 eV, the individual orbital contributions differ (cf. Fig. 3b). The $d_{x^2-y^2}$ dominated DFT band crossing the Fermi level along Γ -X is indeed significantly wider than the d_{z^2} dominated band crossing along X-M. However, the orbital e_g mixing within these bands is still about 2:1 (and vice versa, respectively), due to the reduced energy splitting. As a further interesting aspect, the DFT band structure of tetragonal La_2NiO_4 shows self-doping behavior through a largely La(5d) dominated band creating a small electron pocket around the Z point. This highlights the stronger three-dimensional character compared to e.g. La_2CuO_4 .

The plotted spectral parts and self-energies in Fig. 3 render obvious that within DFT+sicDMFT there is no orbital-selective physics in the tetragonal phase at higher temperature. While indeed the Ni- $d_{x^2-y^2}$ orbital turns out somewhat weaker correlated than the Ni- d_{z^2} one, the gap opening takes place in both orbital sectors also for $U < 10$ eV. Still, the $U = 10$ eV regime appears again best fitting to La_2NiO_4 , as the charge gap results too small for reduced U values. Thus the possible (bad-)metallic behavior at higher temperatures in this compound should be associated with the intriguing defect characteristics at stoichiometry [64, 65].

6. LaNiO_2

The infinite-layer LaNiO_2 belongs to the growing family of superconducting nickelates upon thin-film growth and Sr doping [2, 32, 33]. This finding has stimulated a vast theory interest in these type of compounds (see e.g. [18–20, 35, 36, 69–89] among others), with notable earlier work [90, 91]. For a detailed discussion within the DFT+sicDMFT approach for the case of NdNiO_2 , we refer to our previous works [20, 35, 36].

Non-surprisingly, the essential physics of LaNiO_2 far away from the low-temperature regime turns out very similar to NdNiO_2 on the present level of theory. Figure 4a-c display the key features of the paramagnetic electronic spectrum. The DFT density of states describes a good metallic system, yet strong electronic correlations transfer most of the low-energy spectral weight to higher energies. Note

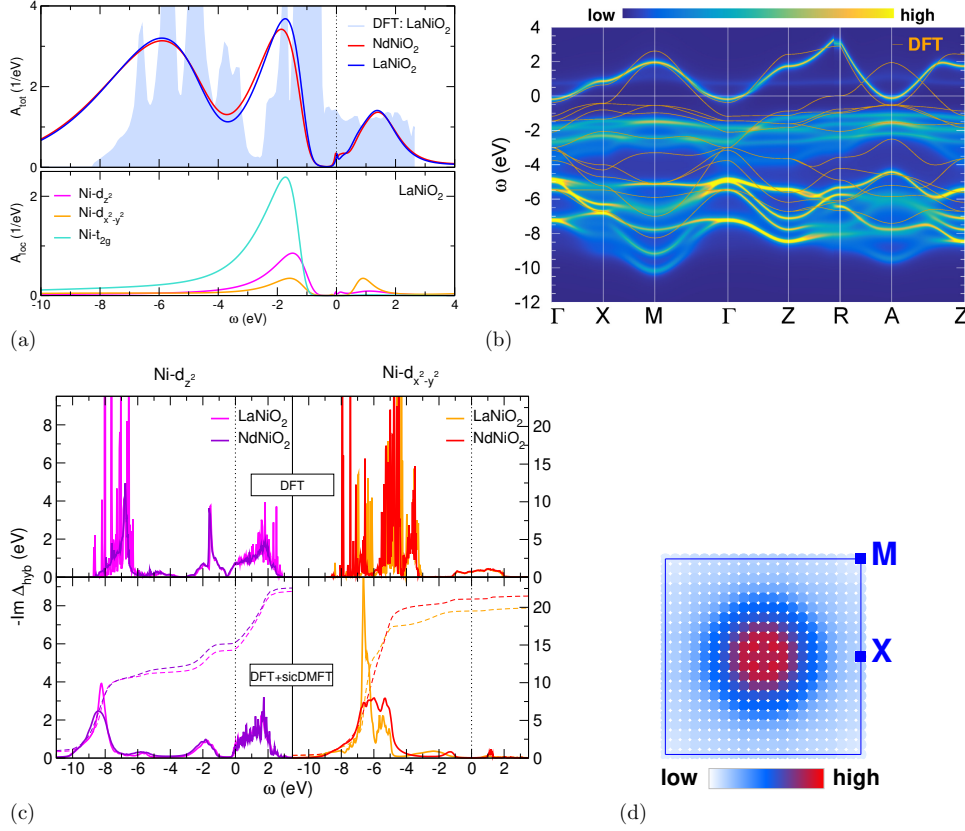


Figure 4. DFT+sicDMFT data for LaNiO₂ ($T = 193$ K). (a) k -integrated total spectrum (top), comparing with the NdNiO₂ total spectrum, and local Ni(3d) spectrum (bottom). (b) k -resolved spectral function with comparison to DFT dispersion. (c) Imaginary part of the Ni- e_g hybridization function displayed as $-\text{Im } \Delta_{\text{hyb}}$ in the DFT limit (top) and in the interacting regime (bottom). (d) Static weak-coupling spin susceptibility $\chi_s(\mathbf{q}, 0)$ for $\mathbf{q} = (q_x, q_y, 0)$.

that the DFT+sicDMFT predicted spectrum agrees well with data from recent photoemission spectroscopy performed on thin films of PrNiO₂ [92], where the two main peaks at -2 eV and -5.5 eV are well confirmed by experiment. The Ni⁺(3d⁹) configuration leads to an intriguing situation where the Ni- $d_{x^2-y^2}$ orbital is close to half filling and residual hole character in the Ni- d_{z^2} orbital remains (cf. Fig. 4a, lower panel). That latter character is achieved via a self-doping band of dominant La(5d) nature, causing electron pockets around the Γ and A point in reciprocal space, which still carry minor Ni- d_{z^2} hybridization weight. Contrary to the self-doping band in tetragonal La₂NiO₄, the electron pockets at the Fermi level survive the impact of strong electronic correlations. Reason is that those pockets do not carry Ni- $d_{x^2-y^2}$ weight and are therefore not shifted to higher energies. Thus the effective Ni- $d_{x^2-y^2}$ band is most-proximate to a (orbital-selective) Mott transition and the largely-filled and therefore weakly-to-moderately correlated Ni- d_{z^2} orbital remains in a joint metallic state with the La(5d) orbitals (see Fig. 4b). For illustration, we also show in Fig. 4c the imaginary diagonal part of the Ni- e_g hybridization

function Δ_{hyb} in the DFT limit [89] as well as in the interacting regime with $\Delta_{\text{hyb}}(\omega) = \omega + \mu - G_{\text{loc}}^{-1}(\omega) - \Sigma_{\text{imp}}(\omega)$. In the DFT limit, both $\text{Ni-}e_g$ have sizable weight at low-energy, whereas the hybridization function for the $\text{Ni-}d_{x^2-y^2}$ vanishes in DFT+sicDMFT close to the Fermi level because of its Mott-insulating nature. The hybridization structures with $\text{O}(2p)$ are dominant at higher energy around -6 eV especially for $\text{Ni-}d_{x^2-y^2}$. Note the energy shift towards deeper energies due to the SIC inclusion compared to standard DFT. Comparing LaNiO_2 and NdNiO_2 does not reveal striking differences in Δ_{hyb} . But it is revealed that the frequency-integrated hybridization (dashed lines in lower panel of Fig. 4c), is somewhat stronger for the Nd compound. This could affect the low-temperature physics in some regard, and different features seem indeed revealed experimentally [32] (see also text below).

Loosely speaking, infinite-layer nickelate with the missing apical oxygen can be viewed as a coupling of two dichotomic subsystems: strongly hybridized/correlated $\text{Ni-}d_{x^2-y^2}\text{-O}(2p)$ and weakly-correlated $\text{Ni-}d_{z^2}\text{-RE}(5d)$. Hole doping leads to a further rise of complexity in the entanglement of these two subsystems, namely a change from (orbital-selective) Mottness to Hundness via the enclosed superconducting region [20, 35, 36]. But we will not pursue this physics in the present context.

Instead, we here want to briefly comment on the issue of ordered magnetism, since the spin physics of RENiO_2 compounds is highly puzzling in experiment. Absence of long-range order [41, 93], quasi-static ordering [94], spin-glass physics [95], pseudogap vs. Curie-Weiss [96] and (para)magnon dispersions [97] are discussed. Various theoretical accounts [84, 85, 98] find a nearest-neighbor superexchange coupling $J \sim 60 - 70\text{ meV}$, i.e. about half the size of the value in high- T_c cuprates, and antiferromagnetic order should thus be favorable. However one must also remember that all available calculations find a metallic state for RENiO_2 at stoichiometry, either due to a robust $\text{Ni-}d_{x^2-y^2}$ quasiparticle weight and/or, as here, because of the existent self-doping band. This is in stark contrast to layered cuprates. But metallicity, strong electronic correlations and AFM order do not go along very well in nature, reason why there are only few reported materials cases (see e.g. discussion in [99]). Furthermore, the stronger three-dimensional character of RENiO_2 compared to layered cuprates does not help either to stabilize AFM order under these circumstances. Therefore given the electronic structure of the infinite-layer nickelates, the absence of robust AFM order in experiment is in fact not totally surprising. To underline this viewpoint, we show in Fig. 4d the diagonal part of the LaNiO_2 static weak-coupling spin susceptibility $\chi_s(\mathbf{q}, 0) = -\frac{1}{\beta} \sum_{\mathbf{k}n, \nu\nu'} G_\nu(\mathbf{k}, i\omega_n) G_{\nu'}(\mathbf{k} + \mathbf{q}, i\omega_n)$, where ω_n are fermionic Matsubara frequencies and G_ν denotes the converged DFT+sicDMFT Green's function in Bloch space for band indices $\nu\nu'$. This simplified Lindhard-like susceptibility neglects vertex contributions and makes only sense in a system with existing low-energy spectral weight. Because of the self-doping electron pockets around Γ and A (plus some very weak leftovers from the effectively Mott-insulating $\text{Ni-}d_{x^2-y^2}$ band), χ_s is nonzero and obviously has highest intensity around Γ . Note that the absolute values are still low and far off any instability regime. Still, the maximum close to the zone centre puts the system in favor of ferromagnetic ordering tendencies from this perspective. These tendencies oppose the strong-coupling AFM tendencies from the superexchange perspective. Again to be clear, we do not at all claim that the given χ_s describes the full range of spin fluctuations in LaNiO_2 adequately, it only shines a light on the implications coming from the metallic side of the problem. Let us also mention that additionally, a unique Kondo scenario involving the $\text{Ni-}d_{x^2-y^2}$ spin and the self-doping band has been detected below $T \sim 60\text{ K}$ for the case of NdNiO_2 [35]. Note that

again the Ni- d_{z^2} orbital, hybridized onto the self-doping band, plays a decisive role in arranging for link between Ni- $d_{x^2-y^2}$ spin and itinerant electrons. It was shown [36], that this Kondo coupling may interfere/coexist with AFM ordering tendencies at low temperatures.

Equipped with our IC scheme to handle finite spin polarization in the interacting regime, the DFT+sicDMFT calculations for most promising C-type AFM order [35, 82, 84], i.e. AFM in-plane and FM out-of-plane, results in ordered Ni moments of size $m_{\text{Ni}} \leq 0.05 \mu_{\text{B}}$. This result holds for $T = 190$ K as well as for the lower-temperature regime of $T = 30$ K. Thus in qualitative agreement with our previous work on NdNiO₂, the tendency to establish sizable-moment antiferromagnetism in RENiO₂ is weak, in agreement with experimental findings. Note that we employed identical initialization protocols with starting moments to eventually stabilize magnetic order, and while the d^8 compound La₂NiO₄ develops substantial Ni moments (see previous section), the d^9 compound LaNiO₂ does not. However, the residual magnetic order apparently helps to establish a stable electronic LaNiO₂ phase at lower temperature $T = 30$ K. In contrast to NdNiO₂ [35, 36], the Ni- d_{z^2} orbital in the PM phase seemingly becomes in some way critical at lower T as the associated self-energy develops unphysical features at small Matsubara frequencies. This might be a numerical artifact, but we still want to report it here, since several careful attempts to cure these features were unsuccessful. One then surely enters highly speculative territory, but the basic message could be that the Kondo-decorated PM phase (and its underlying unconventional Ni- e_g -RE(5d) coupling structure) detected for NdNiO₂, is in some way 'disturbed' in LaNiO₂ at comparable temperatures.

7. Conclusions

In this work we presented a comparison of the correlated electronic structure of three different $3d^n$ nickelates, i.e., formal- d^7 LaNiO₃, d^8 La₂NiO₄ and d^9 LaNiO₂, based on calculations within the DFT+sicDMFT scheme. One goal was to evaluate the performance of the latter scheme for the wider class of nickel-oxide compounds. Moreover, we chose to fix the local Coulomb parameters U and J_{H} to examine if key features of the different compounds can still be well described without fine tuning (or direct calculation) of the interaction integrals. Concerning both aspects, positive results are reported here. The DFT+sicDMFT approach is very capable of describing the correlated-metal nature of LaNiO₃ with its hole on oxygen as well as the Mott-insulating characteristics of La₂NiO₄. And importantly, the constant-interaction strength approach shows that while a detailed knowledge/calculation of the Hubbard parameters is surely a relevant goal, main electronic-structure features are well describable without strong changes of the interaction strength from one compound to another. For the case of LaNiO₂, comparison to experiment remains still difficult due to the scarce availability of measured data. But the present results for the other two compounds and recent photoemission data [92] provide some confidence that the here (and elsewhere [20, 35, 36]) established picture for infinite-layer nickelates will also prove reliable.

In the course of this materials study, a refined scheme to perform spin-polarized DFT+(sic)DMFT studies was introduced. This intermediate-coupling scheme spin averages the DFT charge density terms that connect to the local part of the problem, but still allows for finite spin polarization in the plane-wave-derived charge density within DFT. Hence most of the spin polarization should be generated in the DMFT

part, yet a minor feedback into the DFT part is restored. This new scheme provides ordered Ni moments for La_2NiO_4 in excellent agreement with experiment. It furthermore confirms our recent results [36] of a (nearly) vanishing AFM-ordered Ni moment in infinite-layer nickelates, also in line with experiment. The intriguing metallic(-like) nature at stoichiometry may be blamed for prohibiting a strongly correlated AFM state.

Finally, let us reiterate on the fact that nickelates, in general, are manifest Ni- e_g systems. While for LaNiO_3 , the d_{z^2} and $d_{x^2-y^2}$ orbital act quite coherently, some dichotomy sets in for La_2NiO_4 . Crystal-field splitting and different bandwidths cause orbital differentiation for this layered d^8 compound, but in the end both orbital sectors give rise to similar qualitative behavior. Then for LaNiO_2 this dichotomy is forced to an utmost limit, where half-filled $d_{x^2-y^2}$ is (nearly) Mott-insulating and largely-filled d_{z^2} remains metallic. It is interesting to note that, as shown, orbital selectivity and self-doping character are already a matter of debate for La_2NiO_4 , namely in its high-temperature tetragonal phase. However, these issues apparently only become severe as a 'game changer' for the d^9 LaNiO_2 . In this context it may also be worth to state that the mechanism of getting rid of the DFT self-doping band via rotation/distortion in the orthorhombic phase of La_2NiO_4 , has just been shown to may also be a proper mechanism for later RENiO_2 systems [100,101]. It still has to be explored if the even more extreme dichotomic limit of being able to abandon one of the Ni- e_g orbitals completely from a low-energy discussion can eventually be realized. In any case, the plethora of puzzling and demanding physics that emerges from the Ni- e_g manifold in nickel oxides will remain an exciting research area in condensed matter physics.

Acknowledgments

The author is grateful to A. J. Millis for helpful discussions. Calculations were performed at the Juwels Cluster of the Jülich Supercomputing Centre (JSC) under the hhh08 project.

References

- [1] Mott N F and Peierls R 1937 *Proc. Phys. Soc.* **49** 72
- [2] Li D, Lee K, Wang B Y, Osada M, Crossley S, Lee H R, Cui Y, Hikita Y and Hwang H 2019 *Nature* **572** 624
- [3] Zhang F C and Rice T M 1988 *Phys. Rev. B* **37** 3759(R)
- [4] Imada M, Fujimori A and Tokura Y 1998 *Rev. Mod. Phys.* **70** 1039
- [5] Bednorz J G and Müller K A 1986 *Z. Physik B - Condensed Matter* **64** 189
- [6] Sawatzky G A and Allen J W 1984 *Phys. Rev. Lett.* **53** 2339
- [7] Hüfner S, Osterwalder J, Riesterer T and Hulliger F 1984 *Solid State Comm.* **52** 793
- [8] van der Laan G, Zaanen J, Sawatzky G A, Karnatak R and Esteva J M 1986 *Phys. Rev. B* **33** 4253
- [9] van Elp J, Eskes H, Kuiper P and Sawatzky G A 1992 *Phys. Rev. B* **45** 1612
- [10] Goodenough J B and Ramasesha S 1982 *Mater. Res. Bull.* **17** 383
- [11] Sayer M and Odier P 1987 *J. Solid State Chem.* **67** 26
- [12] Aepli G and Buttrey D J 1988 *Phys. Rev. Lett.* **61** 203
- [13] Guo G Y and Temmerman W M 1988 *J. Phys. C* **21** L917
- [14] Batlle X, Garcia-Muñoz J L, Medarde M, Rodríguez-Carvajal J, Obradors X, Martínez J L, Vallet M, Gonzalez-Calbet J, Sayaguez M J and Fontcuberta J 1989 *Physica C* **162-164** 1273
- [15] Kuiper P, van Elp J, Sawatzky G A, Fujimori A, Hosoya S and de Leeuw D M 1991 *Phys. Rev. B* **44**(9) 4570-4575

- [16] Horiba K, Eguchi R, Taguchi M, Chainani A, Kikkawa A, Senba Y, Ohashi H and Shin S 2007 *Phys. Rev. B* **76**(15) 155104
- [17] Crespin M, Levitz P and Gatinneau L 1983 *J. Chem. Soc., Faraday Trans. 2* **79**(8) 1181–1194
- [18] Nomura Y, Hirayama M, Tadano T, Yoshimoto Y, Nakamura K and Arita R 2019 *Phys. Rev. B* **100** 205138
- [19] Wu X, Sante D D, Schwemmer T, Hanke W, Hwang H Y, Raghu S and Thomale R 2020 *Phys. Rev. B* **101** 060504(R)
- [20] Lechermann F 2020 *Phys. Rev. B* **101** 081110((R))
- [21] Lechermann F, Körner W, Urban D F and Elsässer C 2019 *Phys. Rev. B* **100**(11) 115125
- [22] Savrasov S Y, Kotliar G and Abrahams E 2001 *Nature* **410** 793
- [23] Pourovskii L V, Amadon B, Biermann S and Georges A 2007 *Phys. Rev. B* **76** 235101
- [24] Grieger D, Piefke C, Peil O E and Lechermann F 2012 *Phys. Rev. B* **86** 155121
- [25] Elsässer C, Takeuchi N, Ho K M, Chan C T, Braun P and Fähnle M 1990 *J. Phys.: Condens. Matter* **2** 4371
- [26] Lechermann F, Welsch F, Elsässer C, Ederer C, Fähnle M, Sanchez J M and Meyer B 2002 *Phys. Rev. B* **65** 132104
- [27] Meyer B, Elsässer C, Lechermann F and Fähnle M 1998 *FORTTRAN 90 Program for Mixed-Basis-Pseudopotential Calculations for Crystals* Max-Planck-Institut für Metallforschung, Stuttgart
- [28] Vogel D, Krüger P and Pollmann J 1996 *Phys. Rev. B* **54**(8) 5495–5511
- [29] Filipetti A and Spaldin N A 2003 *Phys. Rev. B* **67** 125109
- [30] Körner W and Elsässer C 2010 *Phys. Rev. B* **81** 085324
- [31] Zhang G M, Yang Y F and Zhang F C 2020 *Phys. Rev. B* **101** 020501(R)
- [32] Osada M, Wang B Y, Goodge B H, Harvey S P, Lee K, Li D, Kourkoutis L F and Hwang H Y 2021 *arXiv:2105.13494*
- [33] Zeng S W, Li C J, Chow L E, Cao Y, Zhang Z T, Tang C S, Yin X M, Lim Z S, Hu J X, Yang P and Ariando A 2021 *arXiv:2105.13492*
- [34] Amadon B, Lechermann F, Georges A, Jollet F, Wehling T O and Lichtenstein A I 2008 *Phys. Rev. B* **77** 205112
- [35] Lechermann F 2020 *Phys. Rev. X* **10** 041002
- [36] Lechermann F 2021 *Phys. Rev. Materials* **5** 044803
- [37] Keshavarz S, Schött J, Millis A J and Kvashnin Y O 2018 *Phys. Rev. B* **97**(18) 184404
- [38] Flesch A, Gorelov E, Koch E and Pavarini E 2013 *Phys. Rev. B* **87**(19) 195141
- [39] Zhang J, Zheng H, Ren Y and Mitchell J F 2017 *Crystal Growth & Design* **17** 2730
- [40] Rodriguez-Carvajal J, Fernandez-Diaz M T and Martinez J L 1991 *Journal of Physics: Condensed Matter* **3** 3215
- [41] Hayward M A, Green M A, Rosseinsky M J and Sloan J 1999 *J. Am. Chem. Soc.* **121** 8843
- [42] Werner P, Comanac A, de' Medici L, Troyer M and Millis A J 2006 *Phys. Rev. Lett.* **97** 076405
- [43] Parcollet O, Ferrero M, Ayrat T, Hafermann H, Krivenko I, Messio L and Seth P 2015 *Comput. Phys. Commun.* **196** 398
- [44] Seth P, Krivenko I, Ferrero M and Parcollet O 2016 *Comput. Phys. Commun.* **200** 274
- [45] Anisimov V I, Solov'yev I V, Korotin M A, Czyżyk M T and Sawatzky G A 1993 *Phys. Rev. B* **48** 16929
- [46] Jarrell M and Gubernatis J E 1996 *Physics Reports* **269**(3) 133
- [47] Vidberg H J and Serene J W 1977 *J Low Temp Phys* **29** 179
- [48] Demourgues A, Weill F, Darriet B, Wattiaux A, Grenier J, Gravereau P and Pouchard M 1993 *Journal of Solid State Chemistry* **106** 330
- [49] Mizokawa T, Khomskii D I and Sawatzky G A 2000 *Phys. Rev. B* **61**(17) 11263–11266
- [50] Park H, Millis A J and Marianetti C A 2012 *Phys. Rev. Lett.* **109**(15) 156402
- [51] Lau B and Millis A J 2013 *Phys. Rev. Lett.* **110**(12) 126404
- [52] Johnston S, Mukherjee A, Elfimov I, Berciu M and Sawatzky G A 2014 *Phys. Rev. Lett.* **112**(10) 106404
- [53] Subedi A, Peil O E and Georges A 2015 *Phys. Rev. B* **91**(7) 075128
- [54] Bisogni V, Catalano S, Green R J, Gibert M, Scherwitsl R, Huang Y, Strocov V N, Zubko P, Balandeh S, Triscone J M, Sawatzky G and Schmitt T 2016 *Nat Commun* **7** 13017
- [55] Eisaki H, Uchida S, Mizokawa T, Namatame H, Fujimori A, van Elp J, Kuiper P, Sawatzky G A, Hosoya S and Katayama-Yoshida H 1992 *Phys. Rev. B* **45**(21) 12513–12521
- [56] Ouellette D G, Lee S, Son J, Stemmer S, Balents L, Millis A J and Allen S J 2010 *Phys. Rev. B* **82**(16) 165112
- [57] Nowadnick E A, Ruf J P, Park H, King P D C, Schlom D G, Shen K M and Millis A J 2015 *Phys. Rev. B* **92**(24) 245109

- [58] Deng X, Ferrero M, Mravlje J, Aichhorn M and Georges A 2012 *Phys. Rev. B* **85**(12) 125137
- [59] Liao X, Singh V and Park H 2021 *Phys. Rev. B* **103**(8) 085110
- [60] Karner V L, Chatzichristos A, Cortie D L, Dehn M H, Foyevtsov O, Foyevtsova K, Fujimoto D, Kiehl R F, Levy C D P, Li R, McFadden R M L, Morris G D, Pearson M R, Stachura M, Ticknor J O, Cristiani G, Logvenov G, Wrobel F, Keimer B, Zhang J, Mitchell J F and MacFarlane W A 2019 *Phys. Rev. B* **100**(16) 165109
- [61] Zhou N, Chen G, Zhang H and Zhou C 2009 *Physica B: Condensed Matter* **404** 4150–4154
- [62] Pardo V, Botana A S and Baldomir D 2012 *Phys. Rev. B* **86**(16) 165114
- [63] Lane C and Zhu J X 2020 *Phys. Rev. B* **101**(15) 155135
- [64] Jorgensen J D, Dabrowski B, Pei S, Richards D R and Hinks D G 1989 *Phys. Rev. B* **40**(4) 2187–2199
- [65] Bassat J, Odier P and Loup J 1994 *Journal of Solid State Chemistry* **110** 124–135
- [66] Lander G H, Brown P J, Spal/ek J and Honig J M 1989 *Phys. Rev. B* **40**(7) 4463–4471
- [67] Ganguly P and Rao C N R 1973 *Mater. Res. Bull.* **8** 405
- [68] Fontcuberta J and Goodenough J 1985 *Journal of Solid State Chemistry* **56** 116–121
- [69] Hu L H and Wu C 2019 *Phys. Rev. Research* **1**(3) 032046
- [70] Jiang M, Berciu M and Sawatzky G A 2020 *Phys. Rev. Lett.* **124** 207004
- [71] Jiang P, Si L, Liao Z and Zhong Z 2019 *Phys. Rev. B* **100**(20) 201106
- [72] Werner P and Hoshino S 2020 *Phys. Rev. B* **101** 041104(R)
- [73] Li D, Wang B Y, Lee K, Harvey S P, Osada M, Goodge B H, Kourkoutis L F and Hwang H Y 2020 *Phys. Rev. Lett.* **125** 027001
- [74] Gu Y, Zhu S, Wang X, Hu J and Chen H 2020 *Commun Phys* **3** 84
- [75] Leonov I, Skorniyakov S L and Savrasov S Y 2020 *Phys. Rev. B* **101** "241108(R)"
- [76] Wang Y, Kang C J, Miao H and Kotliar G 2020 *Phys. Rev. B* **102**(16) 161118
- [77] Hepting M, Li D, Jia C J, Lu H, Paris E, Tseng Y, Feng X, Osada M, Been E, Hikita Y, Chuang Y D, Hussain Z, Zhou K J, Nag A, Garcia-Fernandez M, Rossi M, Huang H Y, Huang D J, Shen Z X, Schmitt T, Hwang H Y, Moritz B, Zaanen J, Devereaux T P and Lee W S 2020 *Nat. Mater.* doi:10.1038/s41563-019-0585-z
- [78] Zhang Y H and Vishwanath A 2020 *Phys. Rev. Research* **2** 023112
- [79] Botana A S and Norman M R 2020 *Phys. Rev. X* **10** 011024
- [80] Si L, Xiao W, Kaufmann J, Tomczak J M, Lu Y, Zhong Z and Held K 2020 *Phys. Rev. Lett.* **124**(16) 166402
- [81] Olevano V, Bernardini F, Blase X and Cano A 2020 *Phys. Rev. B* **101**(16) 161102
- [82] Choi M Y, Pickett W E and Lee K W 2020 *Phys. Rev. Research* **2**(3) 033445
- [83] Karp J, Botana A S, Norman M R, Park H, Zingl M and Millis A 2020 *Phys. Rev. X* **10** 021061
- [84] Zhang R, Lane C, Singh B, Nokelainen J, Barbiellini B, Markiewicz R S, Bansil A and Sun J 2021 *Commun. Phys.* **4** 118
- [85] Katukuri V M, Bogdanov N A, Weser O, van den Brink J and Alavi A 2020 *Phys. Rev. B* **102**(24) 241112
- [86] Been E, Lee W S, Hwang H Y, Cui Y, Zaanen J, Devereaux T, Moritz B and Jia C 2021 *Phys. Rev. X* **11**(1) 011050
- [87] Plienbunrung T, Daghofer M and Oleś A M 2021 *Phys. Rev. B* **103**(10) 104513
- [88] Choubey P and Eremin I M 2021 *Phys. Rev. B* **104**(14) 144504
- [89] Karp J, Hampel A and Millis A J 2021 *Phys. Rev. B* **103**(19) 195101 URL <https://link.aps.org/doi/10.1103/PhysRevB.103.195101>
- [90] Anisimov V I, Bukhvalov D and Rice T M 1999 *Phys. Rev. B* **59**(12) 7901–7906
- [91] Lee K W and Pickett W E 2004 *Phys. Rev. B* **70**(16) 165109
- [92] Chen Z, Osada M, Li D, Been E M, Chen S D, Hashimoto M, Lu D, Mo S K, Lee K, Wang B Y, Rodolakis F, McChesney J L, Jia C, Moritz B, Devereaux T P, Hwang H Y and Shen Z X 2021 *arXiv:2106.03963*
- [93] Wang B X, Zheng H, Krivyakina E, Chmaissem O, Lopes P P, Lynn J W, Gallington L C, Ren Y, Rosenkranz S, Mitchell J F and Phelan D 2020 *Phys. Rev. Materials* **4**(8) 084409
- [94] Cui Y, Li C, Li Q, Zhu X, Hu Z, feng Yang Y, Zhang J S, Yu R, Wen H H and Yu W 2020 *arXiv:2011.09610*
- [95] Lin H, Gawryluk D J, Klein Y M, Huangfu S, Pomjakushina E, von Rohr F and Schilling A 2021 *arXiv:2104.14324*
- [96] Zhao D, Zhou Y B, Fu Y, Wang L, Zhou X F, Cheng H, Li J, Song D W, Li S J, Kang B L, Zheng L X, Nie L P, Wu Z M, Shan M, Yu F H, Ying J J, Wang S M, Mei J W, Wu T and Chen X H 2021 *Phys. Rev. Lett.* **126**(19) 197001
- [97] Lu H, Rossi M, Nag A, Osada M, Li D F, Lee K, Wang B Y, Garcia-Fernandez M, Agrestini S, Shen Z X, Been E M, Moritz B, Devereaux T P, Zaanen J, Zhou H Y H K J and Lee W S

- 2021 *Science* **373** 213
- [98] Wan X, Ivanov V, Resta G, Leonov I and Savrasov S Y 2021 *Phys. Rev. B* **103**(7) 075123
 - [99] Komarek A C, Möller T, Isobe M, Drees Y, Ulbrich H, Azuma M, Fernández-Díaz M T, Senyshyn A, Hoelzel M, André G, Ueda Y, Grüninger M and Braden M 2011 *Phys. Rev. B* **84**(12) 125114
 - [100] Xia C, Wu J, Chen Y and Chen H 2021 *arXiv:2110.12405*
 - [101] Bernardini F, Bosin A and Cano A *arXiv:2110.13580*